

Ridge Estimation with Nonlinear Transformations

Zheng Zhai^{a,c,1}, Hengchao Chen^b, Zhigang Yao^{c,*}

^aInformation Science and Technology College, Dalian Maritime University, China

^bDepartment of Statistical Sciences, University of Toronto, Canada

^cDepartment of Statistics and Data Science, National University of Singapore, Singapore

Abstract

Ridge estimation is an important manifold learning technique. The goal of this paper is to examine the effects of nonlinear transformations on the ridge sets. The main result proves the inclusion relationship between ridges: $\mathcal{R}(f \circ p) \subseteq \mathcal{R}(p)$, provided that the transformation f is strictly increasing and concave on the range of the function p . Additionally, given an underlying true manifold \mathcal{M} , we show that the Hausdorff distance between $\mathcal{R}(f \circ p)$ and its projection onto \mathcal{M} is smaller than the Hausdorff distance between $\mathcal{R}(p)$ and the corresponding projection. This motivates us to apply an increasing and concave transformation before the ridge estimation. In specific, we show that the power transformations $f^q(y) = y^q/q, -\infty < q \leq 1$ are increasing and concave on \mathbb{R}_+ , and thus we can use such power transformations when p is strictly positive. Numerical experiments demonstrate the advantages of the proposed methods.

Keywords: ridge estimation, increasing and concave transformations, inclusion relationship, power transformations.

1. Introduction

Manifold learning is an unsupervised learning technique that aims to uncover the hidden low-dimensional structure within high-dimensional data. It is based

*Corresponding author

¹Part of this work was done when Zheng Zhai worked as a research fellow at National University of Singapore.

on the assumption that real-world high-dimensional data often lie near a lower-dimensional manifold, and thus uncovering this inherent structure can promote data understanding and processing. Manifold learning is in general challenging due to the presence of noise and the infinite flexibility of fitting methods. To leverage the hidden low-dimensional structure, some works propose certain nonlinear dimension reduction methods that enable effective visualization of high-dimensional data [1, 2, 3, 4, 5]. However, these methods do not recover the underlying true manifolds. To recover the inherent manifold structure, some works propose to fit data via local approximation strategies [6, 7, 8]. Some works model the underlying low-dimensional structure as principal curves and surfaces and design suitable estimation methods [9, 10]. Some other research models the underlying manifold as the ridge of the density function and proposes a subspace-constrained mean shift algorithm for the estimation [11, 12]. In this paper, we will focus on the ridge estimation and investigate the effect of nonlinear density transformations on the defined ridge sets.

The ridge of a function represents the higher regions of a function, which generalizes the concept of mode. Mathematically, given a second-order differentiable function $p : \mathbb{R}^D \rightarrow \mathbb{R}$, the d -dimensional ridge of p is given by

$$\mathcal{R}(p) = \{x \mid \lambda_{d+1}(H_p(x)) < 0, \Pi^\perp(H_p(x))\nabla p(x) = 0\}, \quad (1)$$

where $\nabla p(x)$ and $H_p(x)$ represent the gradient and the Hessian matrix of the function p evaluated at the point x , $\Pi^\perp(H_p(x)) = I - \Pi(H_p(x))$ is the projection matrix associated with the last $D - d$ eigenvectors of $H_p(x)$ ². In particular, the mode of a function is exactly its zero dimensional ridge. When the concept of ridge is first proposed in [12], it is used to approximate the underlying manifold structure of the data. By estimating the density function of data and finding the ridge sets, one can either denoise data [13] or perform clustering [14, 15]. Also, some other works treat modes as the response and study modal regression

²The last $D - d$ eigenvectors of $H_p(x)$ represent the eigenvectors associated with the smallest $D - d$ eigenvalues of $H_p(x)$.

problems [16, 17, 18].

In contrast to these works on ridge estimation, our paper aims to investigate the effect of a nonlinear density transformation on the defined ridge sets. Specifically, let $f : \mathbb{R} \rightarrow \mathbb{R}$ be a transformation map that is strictly increasing and concave on the range $p(\mathbb{R}^D)$ of p . Our main result shows that $\mathcal{R}(f \circ p)$ is a subset of $\mathcal{R}(p)$, where $\mathcal{R}(\cdot)$ denotes the d -dimensional ridge of the given function. Furthermore, let \mathcal{M} be an underlying complete manifold and $\mathcal{P}_{\mathcal{M}} : \mathbb{R}^D \rightarrow \mathcal{M}$ be the projection map onto the manifold \mathcal{M} . We also demonstrate that the Hausdorff distance between the ridge $\mathcal{R}(f \circ p)$ and its projection $\mathcal{P}_{\mathcal{M}}(\mathcal{R}(f \circ p))$ is smaller than the Hausdorff distance between the ridge $\mathcal{R}(p)$ and the projection $\mathcal{P}_{\mathcal{M}}(\mathcal{R}(p))$. In the case where $\mathcal{P}_{\mathcal{M}}(\mathcal{R}(f \circ p)) = \mathcal{P}_{\mathcal{M}}(\mathcal{R}(p)) = \mathcal{M}$, the ridge $\mathcal{R}(f \circ p)$ is a better approximation to \mathcal{M} than the ridge $\mathcal{R}(p)$ in the sense that

$$\text{Haus}(\mathcal{R}(f \circ p), \mathcal{M}) \leq \text{Haus}(\mathcal{R}(p), \mathcal{M}),$$

where $\text{Haus}(\mathcal{A}, \mathcal{B}) \stackrel{\text{def}}{=} \max\{\sup_{x \in \mathcal{A}} \inf_{y \in \mathcal{B}} \|x - y\|_2, \sup_{y \in \mathcal{B}} \inf_{x \in \mathcal{A}} \|x - y\|_2\}$ is the Hausdorff distance between \mathcal{A} and \mathcal{B} . This result motivates us to improve ridge approaches for manifold learning by applying a suitable increasing and concave density transformation.

In particular, our paper restricts p to strictly positive functions such that the range $p(\mathbb{R}^D) \subseteq \mathbb{R}_+$. We examine a sequence of power transformations $f^q : \mathbb{R}_+ \rightarrow \mathbb{R}$, $f^q(y) = y^q/q$, where $-\infty < q \leq 1$ ³. We show that all such power transformations are strictly increasing and concave on \mathbb{R}_+ . Thus, our main result implies that $\mathcal{R}(f^q \circ p) \subseteq \mathcal{R}(p)$. Moreover, we investigate the relationship between different power transformations and find that $\mathcal{R}(f^{q_1} \circ p) \subseteq \mathcal{R}(f^{q_2} \circ p)$ for all $q_1 \leq q_2 \leq 1$. Finally, we study the limit of the ridge set $\mathcal{R}(f^q \circ p)$ when q tends to $-\infty$. We find that

$$\mathcal{R}(f^{-\infty} \circ p) = \lim_{q \rightarrow -\infty} \mathcal{R}(f^q \circ p) = \{x \mid \nabla p(x) = 0, \lambda_{d+1}(H_p(x)) < 0\},$$

which is apparently a subset of the mode of p . In this manner, we provide an

³When $q = 0$, this map is reduced to the logarithm map by L'Hôpital's rule.

annealing view of the ridge sets $\mathcal{R}(f^q \circ p)$ from the original ridge $\mathcal{R}(p)$ to the ridge $\mathcal{R}(f^{-\infty} \circ p)$. Motivated by this, we propose to improve the ridge estimation by choosing a suitable q and estimating the ridge $\mathcal{R}(f^q \circ p)$ instead of $\mathcal{R}(p)$. Our numerical experiments demonstrate the feasibility of this idea.

The rest of this paper is organized as follows. We first present the intuitions behind nonlinear transformations and then rigorously prove the main theorems in Section 2. Next, we consider the density ridge estimation problem and investigate the effects of a sequence of power transformations in Section 3. Numerical experiments are provided in Section 4 and we conclude the paper with some remarks in Section 5.

2. Ridge Estimation with Nonlinear Density Transformation

In this section, we investigate the variations of ridges after applying nonlinear transformations. Recall that the d -dimensional ridge of a second-order differentiable function is defined in (1), which is determined by the first two order derivatives of the function. Let $p : \mathbb{R}^D \rightarrow \mathbb{R}$ be a second-order differentiable function and $f : \mathbb{R} \rightarrow \mathbb{R}$ be a second-order differentiable transformation map. To examine the relationship between ridges⁴ $\mathcal{R}(f \circ p)$ and $\mathcal{R}(p)$, we proceed by studying the gradient and the Hessian matrix of $f \circ p$ as follows:

$$\begin{aligned}\nabla(f \circ p)(x) &= f'(p(x))\nabla p(x), \\ H_{f \circ p}(x) &= f'(p(x)) \cdot H_p^f(x),\end{aligned}$$

where

$$H_p^f(x) = H_p(x) + \frac{f''(p(x))}{f'(p(x))} \nabla p(x) \nabla p^T(x).$$

When f is strictly increasing on the range of p , that is, $f'(p(x)) > 0$, the gradient $\nabla(f \circ p)(x)$ and $\nabla p(x)$ are parallel to each other, and the matrix $H_{f \circ p}(x)$ and $H_p^f(x)$ share the same eigenspace. In particular, let $\Pi_{H_{f \circ p}}(x)$ and $\Pi_{H_p}(x)$ be

⁴We shall abbreviate d -dimensional ridges simply as ridges in this paper.

the projections matrices associated with the leading d eigenvectors of $H_{f \circ p}(x)$ and $H_p(x)$, respectively, then $\Pi_{H_{f \circ p}}(x) = \Pi_{H_p}(x)$. When f is further strictly concave on the range of p , that is, $f''(p) < 0$, the matrix $H_p^f(x)$ is equal to $H_p(x)$ plus a positive semi-definite rank-one matrix $-\lambda uu^T$, where $\lambda = \frac{-f''(p(x))}{f'(p(x))} > 0$ and $u = \nabla p(x)$. Our main theorem is to show that $\mathcal{R}(f \circ p) \subseteq \mathcal{R}(p)$, provided that f is both strictly increasing and concave on the range of p . In other words, we will show that for any $x \in \mathcal{R}(f \circ p)$,

$$(1) \Pi_{H_p}^\perp(x) \nabla p(x) = 0, \quad (2) \lambda_{d+1}(H_p(x)) < 0,$$

where $\Pi_{H_p}^\perp(x) = I - \Pi_{H_p}(x)$ is the projection matrix associated with the last $D-d$ eigenvectors of $H(x)$. To prove this, we need to first establish two lemmas studying the effect of rank-one modification on a symmetric matrix.

Let $B \in \mathbb{R}^{D \times D}$ be a symmetric matrix and $A = B + \lambda uu^T$ be a rank-one modified matrix of B . Lemma 1 shows that if $\lambda \geq 0$, then the leading d eigenspace of A is biased towards u in the sense that $\|\Pi_A u\|_2 \geq \|\Pi_B u\|_2$, where Π_A and Π_B are the projection matrices associated with the top d eigenvectors of A and B .

Lemma 1. *Let $B \in \mathbb{R}^{D \times D}$ be a symmetric matrix and $A = B + \lambda uu^T$ for some $\lambda \geq 0$ and $u \in \mathbb{R}^D$. Then we have $\|\Pi_A u\|_2 \geq \|\Pi_B u\|_2$, where Π_A and Π_B are the projection matrices associated with the leading d eigenvectors of A and B , respectively.*

Proof. By the variational characterization, the top d eigenvectors $U_A \in \mathbb{R}^{D \times d}$ of A are given by

$$U_A = \operatorname{argmax}_{U^T U = I_d} \operatorname{tr}(U^T A U).$$

The trace term can be rewritten as follows:

$$\operatorname{tr}(U^T A U) = \operatorname{tr}(U U^T A) = \langle U U^T, A \rangle.$$

In particular, we have $\operatorname{tr}(U_A^T A U_A) = \langle \Pi_A, A \rangle$, where $\Pi_A = U_A U_A^T$ is the projection matrix associated with U_A . Similarly, the top d eigenvectors $U_B \in \mathbb{R}^{D \times d}$

of B satisfies

$$U_B = \operatorname{argmax}_{U^T U = I_d} \operatorname{tr}(U^T B U).$$

Moreover, $\operatorname{tr}(U_B^T B U_B) = \langle \Pi_B, B \rangle$, where $\Pi_B = U_B U_B^T$ is the projection matrix associated with U_B . By the variational characterization of the eigenvectors of A and B , we obtain $\langle \Pi_A, A \rangle \geq \langle \Pi_B, A \rangle$ and $\langle \Pi_B, B \rangle \geq \langle \Pi_A, B \rangle$. Now since $A = B + \lambda u u^T$, we have

$$\begin{aligned} \langle \Pi_A, A \rangle &= \langle \Pi_A, B \rangle + \langle \Pi_A, \lambda u u^T \rangle \\ &\geq \langle \Pi_B, A \rangle = \langle \Pi_B, B \rangle + \langle \Pi_B, \lambda u u^T \rangle \\ &\geq \langle \Pi_A, B \rangle + \langle \Pi_B, \lambda u u^T \rangle. \end{aligned}$$

Eliminating the term $\langle \Pi_A, B \rangle$ on both sides yields $\langle \Pi_A, u u^T \rangle \geq \langle \Pi_B, u u^T \rangle$. Note that $\|\Pi_A u\|_2^2 = \langle \Pi_A, u u^T \rangle$ and $\|\Pi_B u\|_2^2 = \langle \Pi_B, u u^T \rangle$. Then the lemma immediately follows. \square

Let \mathcal{S}_B^d be the subspace spanned by the leading d eigenvectors of B . Lemma 2 shows that if $\lambda \geq 0$ and $u \in \mathcal{S}_B^d$, then modifying B with a positive semi-definite rank-one matrix $\lambda u u^T$ would not change its remaining $D - d$ eigenvalues.

Lemma 2. *Let $B \in \mathbb{R}^{D \times D}$ be a symmetric matrix and \mathcal{S}_B^d be the subspace spanned by the leading d eigenvectors of B . Let $A = B + \lambda u u^T$ for some $\lambda \geq 0$ and $u \in \mathcal{S}_B^d$. Then the $(d+1)$ to D -th largest eigenvalues of A and B are equal, that is, $\lambda_k(A) = \lambda_k(B)$, $\forall d+1 \leq k \leq D$.*

Proof. By the eigenvalue decomposition, we have

$$B = [U_d, U_{D-d}] \begin{bmatrix} \Lambda^{(1)} & \mathbf{0} \\ \mathbf{0} & \Lambda^{(2)} \end{bmatrix} [U_d, U_{D-d}]^T, \quad (2)$$

where U_d, U_{D-d} denote the leading d and the last $D - d$ eigenvectors of B , and $\Lambda^{(1)}, \Lambda^{(2)}$ collect the leading d and the last $D - d$ eigenvalues of B . Our aim is to show that the last $D - d$ eigenvalues of $A = B + \lambda u u^T$ are equal to $\Lambda^{(2)}$, where $\lambda \geq 0$ and $u \in \mathcal{S}_B^d = \operatorname{span}(U_d)$.

First, since $u \in \mathcal{S}_B^d$, we can write $u = U_d \alpha$ for some $\alpha \in \mathbb{R}^d$. Thus, we have

$$A = B + \lambda u u^T = [U_d, U_{D-d}] \begin{bmatrix} \Lambda^{(1)} + \lambda \alpha \alpha^T & \mathbf{0} \\ \mathbf{0} & \Lambda^{(2)} \end{bmatrix} [U_d, U_{D-d}]^T.$$

By the eigenvalue decomposition, we have

$$\Lambda^{(1)} + \lambda \alpha \alpha^T = P_d \tilde{\Lambda}^{(1)} P_d^T,$$

where $P_d \in \mathbb{R}^{d \times d}$ is an orthogonal matrix and $\tilde{\Lambda}^{(1)}$ contains the eigenvalues of $\Lambda^{(1)} + \lambda \alpha \alpha^T$ in the decreasing order. Let $\tilde{U}_d = U_d P_d$. We have

$$A = [\tilde{U}_d, U_{D-d}] \begin{bmatrix} \tilde{\Lambda}^{(1)} & \mathbf{0} \\ \mathbf{0} & \Lambda^{(2)} \end{bmatrix} [\tilde{U}_d, U_{D-d}]^T. \quad (3)$$

To prove the lemma, it suffices to show that (3) indeed gives the eigenvalue decomposition of A . Specifically, it suffices to show that diagonal values of $\tilde{\Lambda}^{(1)}$ are larger than that of $\Lambda^{(2)}$. In fact, by the Weyl's theorem [19] and the positive semi-definiteness of $\lambda \alpha \alpha^T$, we have $\tilde{\Lambda}_{ii}^{(1)} \geq \Lambda_{ii}^{(1)} \geq \Lambda_{jj}^{(2)}$ for any $i \leq d$ and $j \leq D - d$. This completes the proof of the lemma. \square

By utilizing Lemma 1 and Lemma 2, we can establish the inclusion relationship $\mathcal{R}(f \circ p) \subseteq \mathcal{R}(p)$, given that f is strictly increasing and concave on the range of p .

Theorem 3. *Let $p : \mathbb{R}^D \rightarrow \mathbb{R}$ be a second-order differentiable function and we denote its range by $p(\mathbb{R})$. Suppose the transformation map $f : \mathbb{R} \rightarrow \mathbb{R}$ is strictly increasing and concave on an open interval containing $p(\mathbb{R})$. Then we have $\mathcal{R}(f \circ p) \subseteq \mathcal{R}(p)$, where $\mathcal{R}(\cdot)$ is the d -dimensional ridge of the given function.*

Proof. Recall that the gradient and the Hessian matrix of $f \circ p$ are given by

$$\begin{aligned} \nabla(f \circ p)(x) &= f'(p(x)) \nabla p(x), \\ H_{f \circ p}(x) &= f'(p(x)) \cdot H_p^f(x), \end{aligned}$$

where

$$H_p^f(x) = H_p(x) + \frac{f''(p(x))}{f'(p(x))} \nabla p(x) \nabla p^T(x).$$

The gradient $\nabla(f \circ p)(x)$ is parallel to $\nabla p(x)$. Since $f'(p(x)) > 0$, the eigenvectors of $H_{f \circ p}(x)$ are exactly given by the eigenvectors of $H_p^f(x)$. In particular, $\Pi_{H_p^f}(x) = \Pi_{H_{f \circ p}}(x)$, where $\Pi_{H_p^f}(x)$ and $\Pi_{H_{f \circ p}}(x)$ are the projection matrices associated with the top d eigenvectors of $H_p^f(x)$ and $H_{f \circ p}(x)$, respectively. Since $\frac{f''(p(x))}{f'(p(x))} < 0$, by Lemma 1, we have

$$\|\Pi_{H_{f \circ p}}(x)\nabla p(x)\|_2 = \|\Pi_{H_p^f}(x)\nabla p(x)\|_2 \leq \|\Pi_{H_p}(x)\nabla p(x)\|_2, \quad (4)$$

where $\Pi_{H_p}(x)$ is the projection matrix associated with the leading d eigenvectors of $H_p(x)$. By the Pythagorean theorem, we have

$$\|\nabla p(x)\|_2^2 = \|\Pi_{H_p}^\perp(x)\nabla p(x)\|_2^2 + \|\Pi_{H_p}(x)\nabla p(x)\|_2^2, \quad (5)$$

$$\|\nabla p(x)\|_2^2 = \|\Pi_{H_{f \circ p}}^\perp(x)\nabla p(x)\|_2^2 + \|\Pi_{H_{f \circ p}}(x)\nabla p(x)\|_2^2, \quad (6)$$

where $\Pi_{H_p}^\perp(x) = I - \Pi_{H_p}(x)$ and $\Pi_{H_{f \circ p}}^\perp(x) = I - \Pi_{H_{f \circ p}}(x)$ represent the projection matrices associated with the last $D - d$ eigenvectors of $H_p(x)$ and $H_{f \circ p}(x)$, respectively. Thus, by combining (4), (5), and (6), we have

$$\|\Pi_{H_p}^\perp(x)\nabla p(x)\|_2 \leq \|\Pi_{H_{f \circ p}}^\perp(x)\nabla p(x)\|_2, \quad \forall x.$$

In particular, $\|\Pi_{H_p}^\perp(x)\nabla p(x)\|_2 \leq \|\Pi_{H_{f \circ p}}^\perp(x)\nabla p(x)\|_2 = 0$ for any $x \in \mathcal{R}(f \circ p)$. Therefore, to show that $\mathcal{R}(f \circ p) \subseteq \mathcal{R}(p)$, it remains to show that $\lambda_{d+1}(H_p(x)) < 0$ for any $x \in \mathcal{R}(f \circ p)$. In fact, by Lemma 2 and the facts that $\nabla p(x) \in \mathcal{S}_{f \circ p}(x)$, $\frac{f''(p(x))}{f'(p(x))} < 0$, and $f'(p(x)) > 0$, we have

$$\lambda_{d+1}(H_p(x)) = \lambda_{d+1}(H_p^f(x)) = \frac{1}{f'(p(x))} \lambda_{d+1}(H_{f \circ p}(x)) < 0, \quad \forall x \in \mathcal{R}(f \circ p),$$

which concludes the proof. \square

In manifold learning, the ridge of a function p is used to approximate an underlying manifold $\mathcal{M} \subseteq \mathbb{R}^D$. Suppose \mathcal{M} is a complete manifold and $\mathcal{P}_{\mathcal{M}} : \mathbb{R}^D \rightarrow \mathcal{M}$ is the projection onto the manifold \mathcal{M} . Our next theorem shows that the Hausdorff distance between the ridge $\mathcal{R}(f \circ p)$ and its projection $\mathcal{P}_{\mathcal{M}}(\mathcal{R}(f \circ p))$ is smaller than the Hausdorff distance between the ridge $\mathcal{R}(p)$ and its projection $\mathcal{P}_{\mathcal{M}}(\mathcal{R}(p))$, provided that f is strictly increasing and concave.

Theorem 4. *Let $p : \mathbb{R}^D \rightarrow \mathbb{R}$ be a second-order differentiable function. Suppose the transformation map $f : \mathbb{R} \rightarrow \mathbb{R}$ is strictly increasing and concave on an open interval containing the range $p(\mathbb{R})$ of p . Let $\mathcal{R}(\cdot)$ denote the d -dimensional ridge of the given function. Suppose \mathcal{M} is a complete manifold and $\mathcal{P}_{\mathcal{M}}$ is the projection map onto \mathcal{M} . Then we have*

$$\text{Haus}(\mathcal{R}(f \circ p), \mathcal{P}_{\mathcal{M}}(\mathcal{R}(f \circ p))) \leq \text{Haus}(\mathcal{R}(p), \mathcal{P}_{\mathcal{M}}(\mathcal{R}(p))), \quad (7)$$

Proof. First, let us show the following claim:

$$\text{Haus}(\mathcal{A}, \mathcal{P}_{\mathcal{M}}(\mathcal{A})) = \sup_{x \in \mathcal{A}} \inf_{y \in \mathcal{P}_{\mathcal{M}}(\mathcal{A})} \|x - y\|_2 \quad (8)$$

for any $\mathcal{A} \subseteq \mathbb{R}^D$. In fact, the Hausdorff distance is by definition given by

$$\text{Haus}(\mathcal{A}, \mathcal{P}_{\mathcal{M}}(\mathcal{A})) = \max\{\sup_{x \in \mathcal{A}} \inf_{y \in \mathcal{P}_{\mathcal{M}}(\mathcal{A})} \|x - y\|_2, \sup_{y \in \mathcal{P}_{\mathcal{M}}(\mathcal{A})} \inf_{x \in \mathcal{A}} \|x - y\|_2\}.$$

To prove (8), it suffices to show that

$$\sup_{y \in \mathcal{P}_{\mathcal{M}}(\mathcal{A})} \inf_{x \in \mathcal{A}} \|x - y\|_2 \leq \sup_{x \in \mathcal{A}} \inf_{y \in \mathcal{P}_{\mathcal{M}}(\mathcal{A})} \|x - y\|_2,$$

which is equivalent to proving

$$\inf_{x \in \mathcal{A}} \|x - z\|_2 \leq \sup_{x \in \mathcal{A}} \inf_{y \in \mathcal{P}_{\mathcal{M}}(\mathcal{A})} \|x - y\|_2, \quad \forall z \in \mathcal{P}_{\mathcal{M}}(\mathcal{A}). \quad (9)$$

By definition of $\mathcal{P}_{\mathcal{M}}(\mathcal{A})$, for any $z \in \mathcal{P}_{\mathcal{M}}(\mathcal{A})$, there exists $x_z \in \mathcal{A}$ such that $\|x_z - z\|_2 = \inf_{y \in \mathcal{M}} \|x_z - y\|_2$. Therefore,

$$\begin{aligned} \inf_{x \in \mathcal{A}} \|x - z\|_2 &\leq \|x_z - z\|_2 \\ &= \inf_{y \in \mathcal{M}} \|x_z - y\|_2 \stackrel{(i)}{=} \inf_{y \in \mathcal{P}_{\mathcal{M}}(\mathcal{A})} \|x_z - y\|_2 \\ &\leq \sup_{x \in \mathcal{A}} \inf_{y \in \mathcal{P}_{\mathcal{M}}(\mathcal{A})} \|x - y\|_2, \end{aligned}$$

where (i) holds because $x_z \in \mathcal{A}$. This proves (9) and thus the claim (8).

Now we proceed to prove the theorem. By Theorem 3, we know $\mathcal{R}(f \circ p) \subseteq \mathcal{R}(p)$. As a result, it remains to show the following inequality:

$$\text{Haus}(\mathcal{A}, \mathcal{P}_{\mathcal{M}}(\mathcal{A})) \leq \text{Haus}(\mathcal{B}, \mathcal{P}_{\mathcal{M}}(\mathcal{B}))$$

for any $\mathcal{A} \subseteq \mathcal{B} \subseteq \mathbb{R}^D$. By the claim (8), it suffices to show that

$$\sup_{x \in \mathcal{A}} \inf_{y \in \mathcal{P}_{\mathcal{M}}(\mathcal{A})} \|x - y\|_2 \leq \sup_{x \in \mathcal{B}} \inf_{y \in \mathcal{P}_{\mathcal{M}}(\mathcal{B})} \|x - y\|_2. \quad (10)$$

This is because by definition of $\mathcal{P}_{\mathcal{M}}$,

$$\inf_{y \in \mathcal{P}_{\mathcal{M}}(\mathcal{A})} \|x - y\|_2 = \inf_{y \in \mathcal{M}} \|x - y\|_2 \leq \inf_{y \in \mathcal{P}_{\mathcal{M}}(\mathcal{B})} \|x - y\|_2, \quad \forall x \in \mathcal{A}.$$

Then (10) immediately follows from $\mathcal{A} \subseteq \mathcal{B}$, which concludes the proof. \square

Theorem 4 is especially useful in the case where $\mathcal{P}_{\mathcal{M}}(\mathcal{R}(f \circ p)) = \mathcal{P}_{\mathcal{M}}(\mathcal{R}(p)) = \mathcal{M}$. This situation means the projections of both $\mathcal{R}(f \circ p)$ and $\mathcal{R}(p)$ onto \mathcal{M} are surjective, i.e., \mathcal{M} . Thus, it is better to use $\mathcal{R}(f \circ p)$ as the approximation to the underlying manifold \mathcal{M} . More specifically, we have the following corollary.

Corollary 5. *Under the assumptions of Theorem 4 and an additional condition $\mathcal{P}_{\mathcal{M}}(\mathcal{R}(f \circ p)) = \mathcal{P}_{\mathcal{M}}(\mathcal{R}(p)) = \mathcal{M}$, we have*

$$\text{Haus}(\mathcal{R}(f \circ p), \mathcal{M}) \leq \text{Haus}(\mathcal{R}(p), \mathcal{M}).$$

The above results suggest us to leverage a suitable increasing and concave transformation f and estimate the transformed ridge $\mathcal{R}(f \circ p)$ instead of $\mathcal{R}(p)$. Examples of such transformation functions will be provided in the next section.

3. Power Transformations

In this section, we shall restrict p to the class of strictly positive functions, i.e., $p(\mathbb{R}^D) \subseteq \mathbb{R}_+$. This is the usual case in density ridge estimation where p is given by the kernel density estimate of the data distribution. The objective of this section is to examine a sequence of power transformations $f^q(y) = y^q/q$, $-\infty < q \leq 1$ on the strictly positive functions. Our first main result is the following corollary, which establishes a nested inclusion relationship between ridges using different power transformations.

Corollary 6. *For any $q_1 \leq q_2 \leq 1$, we have*

$$\mathcal{R}(f^{q_1} \circ p) \subseteq \mathcal{R}(f^{q_2} \circ p). \quad (11)$$

In particular, for any $q_1 < 0 < q_2 < 1$, we have

$$\mathcal{R}(f^{q_1} \circ p) \subseteq \mathcal{R}(\log(p)) \subseteq \mathcal{R}(f^{q_2} \circ p) \subseteq \mathcal{R}(p).$$

Proof. Notice that $f^1(y) = y$ is the identify function and $f^0(y) = \log(y)$ is the logarithm map, thus it suffices to show (11). For any $q_1 < q_2 \leq 1$, we observe that $f^{q_1}(y) = g(z) = \frac{1}{q_1} \cdot (q_2 z)^{\frac{q_1}{q_2}}$, where $z = f^{q_2}(y)$ and $y > 0$. When q_1 or q_2 equals zero, the function $g(z)$ is given by L'Hospital's rule. Take derivative of g , we get

$$g'(z) = \frac{q_1}{q_2} \cdot \frac{q_2^{\frac{q_1}{q_2}}}{z^{\frac{q_1}{q_2}-1}} = y^{q_1-q_2} > 0, \quad (12)$$

where the second equality uses $z = f^{q_2}(y)$. Calculating the second order derivative of g , we get

$$g''(z) = \frac{q_1}{q_2} \cdot \frac{q_1 - q_2}{q_2} \cdot z^{\frac{q_1}{q_2}-2} = (q_1 - q_2) \cdot y^{q_1-2q_2} < 0,$$

where we again use $z = f^{q_2}(y)$ and $y > 0$. Therefore, g is strictly increasing and concave on the range of $f^{q_2} \circ p$. The corollary then follows from Theorem 3. \square

Corollary 6 states that when q is smaller, then the ridge $\mathcal{R}(f^q \circ p)$ is a smaller set. This motivates us to study the limit of ridge $\mathcal{R}(f^q \circ p)$ when q tends to $-\infty$. In the following theorem, we show that such limiting ridge is a subset of the mode of the function p .

Theorem 7. *The limit of ridges $\mathcal{R}(f^q \circ p)$ when q tends to $-\infty$ is given by*

$$\mathcal{R}(f^{-\infty} \circ p) = \lim_{q \rightarrow -\infty} \mathcal{R}(f^q \circ p) = \{x \mid \nabla p(x) = 0, \lambda_{d+1}(H_p(x)) < 0\}.$$

where $H_p(x)$ is the Hessian matrix of p evaluated at x .

Proof. First, it is easy to check that

$$\{x \mid \nabla p(x) = 0, \lambda_{d+1}(H_p(x)) < 0\} \subseteq \mathcal{R}(f^q \circ p), \quad \forall q \leq 1.$$

Let q tend to $-\infty$, we obtain

$$\{x \mid \nabla p(x) = 0, \lambda_{d+1}(H_p(x)) < 0\} \subseteq \lim_{q \rightarrow -\infty} \mathcal{R}(f^q \circ p).$$

On the other hand, the Hessian matrix of $f^q \circ p$ is given by

$$H_{f^q \circ p}(x) = (1 - q)p^{q-2}(x) \cdot \left(\frac{p(x)H_p(x)}{1 - q} - \nabla p(x)\nabla p^T(x) \right).$$

The ridge $\mathcal{R}(f^q \circ p)$ is given by

$$\mathcal{R}(f^q \circ p) = \{x \mid \Pi_{H_{f^q \circ p}}^\perp(x)\nabla p(x) = 0, \lambda_{d+1}(H_{f^q \circ p}(x)) < 0\},$$

where $\Pi_{H_{f^q \circ p}}^\perp(x)$ is the projection matrix associated with the last $D - d$ eigenvectors of $H_{f^q \circ p}(x)$. Let e^q be the last eigenvector of $H_{f^q \circ p}(x)$. Then we have $(e^q)^T \nabla p(x) = 0$ for all $x \in \mathcal{R}(f^q \circ p)$. Notice that e^q is also the last eigenvector of

$$H^q(x) = \frac{p(x)H_p(x)}{1 - q} - \nabla p(x)\nabla p^T(x).$$

By the perturbation theory [20], when q tends to $-\infty$, the last eigenvector e^q of H^q converges to the direction of $\nabla p(x)$. When q tends to $-\infty$, $|(e^q)^T \nabla p(x)|$ tends to $\|\nabla p(x)\|_2$, which implies that $\nabla p(x) = 0$ in the limit. This proves that

$$\lim_{q \rightarrow -\infty} \mathcal{R}(f^q \circ p) \subseteq \{x \mid \nabla p(x) = 0, \lambda_{d+1}(H_p(x)) < 0\},$$

which concludes the proof. \square

Comparing this limiting ridge with the mode, $\{x \mid \nabla p(x) = 0, \lambda_1(H_p(x)) < 0\}$, we find that they only differ in the requirement of eigenvalues of $H_p(x)$. In particular, the limiting ridge $\mathcal{R}(f^{-\infty} \circ p)$ is a subset of the mode. Corollary 6 and Theorem 7 provide an annealing picture of ridges $\mathcal{R}(f^q \circ p)$ from the original d -dimensional ridge $\mathcal{R}(p)$ to the mode of p .

3.1. Illustration of power transformations

In this subsection, we will provide three examples to illustrate the effects of power transformations.

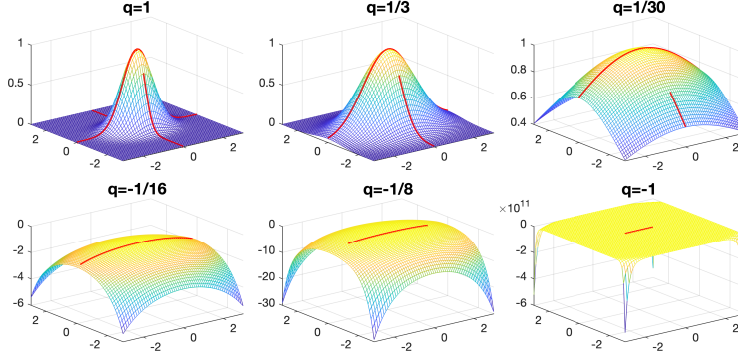


Figure 1: Visualizations of one-dimensional ridges of $f^q \circ p$, $q \in \{1, \frac{1}{3}, \frac{1}{30}, -\frac{1}{16}, -\frac{1}{8}, -1\}$, where $p(x) = \exp(-x_1^2 - 2x_2^2)$. The ridges are plotted as red lines.

3.1.1. Two analytic examples

We first present two analytic examples, where the transformed ridges can be expressed in an analytic way. The first example discusses a unimodal function and the second example involves a bimodal function.

Example 8 (Unimodal function). Consider the function $p(x) = \exp(-x_1^2 - 2x_2^2)$ with $x = (x_1, x_2) \in \mathbb{R}^2$. The gradient and Hessian of $f^q \circ p$ are given by

$$\begin{aligned} \nabla(f^q \circ p)(x) &= 2p^q(x) \cdot [-x_1, -2x_2]^T, \\ H_{f^q \circ p}(x) &= 4p^q(x) \cdot \left(\begin{bmatrix} -1/2 & 0 \\ 0 & -1 \end{bmatrix} + q \begin{bmatrix} x_1^2 & 2x_1x_2 \\ 2x_1x_2 & 4x_2^2 \end{bmatrix} \right). \end{aligned}$$

When $q = 0$, the Hessian matrix is a diagonal matrix and thus it is easy to show that the one-dimensional ridge of $f^0 \circ p$ is given by

$$\mathcal{R}(f^0 \circ p) = \{(x_1, 0) \mid x_1 \in \mathbb{R}\}.$$

When $q < 0$, Corollary 6 implies that $\mathcal{R}(f^q \circ p) \subseteq \mathcal{R}(f^0 \circ p)$, and thus we only need to consider the case where $x_2 = 0$. The Hessian matrix is again a diagonal matrix and we can show by definition that the ridge $\mathcal{R}(f^q \circ p)$ is given by

$$\mathcal{R}(f^q \circ p) = \{(x_1, 0) \mid x_1^2 < -\frac{1}{2q}\}, \quad q < 0.$$

When $0 < q \leq 1$, Corollary 6 implies that $\mathcal{R}(f^0 \circ p) \subseteq \mathcal{R}(f^q \circ p)$. Therefore, we only need to consider the case where $x_2 \neq 0$. First, we suppose $x_1 = 0$ when the

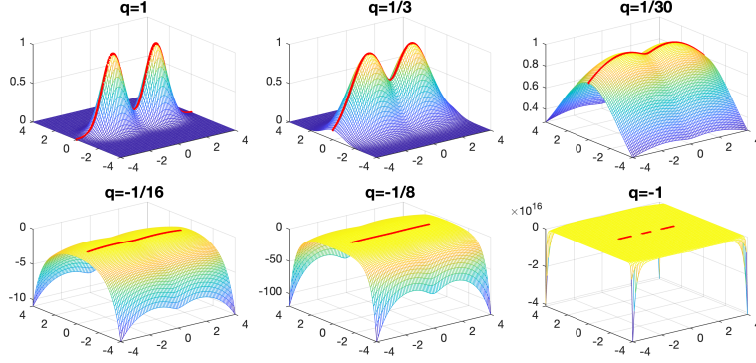


Figure 2: Visualization of one-dimensional ridge of $f^q \circ p$, $q \in \{1, \frac{1}{3}, \frac{1}{30}, -\frac{1}{16}, -\frac{1}{8}, -1\}$, where $p(x) = \exp(-(x_1 - 1.5)^2 - 2x_2^2) + \exp(-(x_1 + 1.5)^2 - 2x_2^2)$. The ridges are plotted as red lines.

Hessian is again a diagonal matrix. We can show by definition that

$$\{(0, x_2) \mid x_2^2 > \frac{1}{4q}\} = \mathcal{R}(f^q \circ p) \cap \{(0, x_2) \mid x_2 \in \mathbb{R}\}.$$

Next, we consider the case where $x_1 \neq 0, x_2 \neq 0$. In this case, the eigenspace of

$$q \begin{bmatrix} x_1^2 & 2x_1x_2 \\ 2x_1x_2 & 4x_2^2 \end{bmatrix} = q \begin{bmatrix} x_1 \\ 2x_2 \end{bmatrix} \begin{bmatrix} x_1 \\ 2x_2 \end{bmatrix}^T$$

is perturbed by the diagonal matrix $\text{diag}(-1/2, 1)$. In particular, all eigenvectors of $H_{f^q \circ p}(x)$ are not parallel to $[-x_1, -2x_2]^T$. This implies that $\nabla(f^q \circ p)(x)$ is not vanished in the space spanned by the last eigenvector of $H_{f^q \circ p}(x)$ and thus $x = (x_1, x_2) \notin \mathcal{R}(f^q \circ p)$. Combining all the results, we show that

$$\mathcal{R}(f^q \circ p) = \{(x_1, 0) \mid x_1 \in \mathbb{R}\} \cup \{(0, x_2) \mid x_2^2 \geq \frac{1}{4q}\}, \quad 0 < q \leq 1.$$

Figure 1 visualizes ridges of p with different power transformations f^q .

Example 9 (Bimodal function). *Consider the bimodal function $p(x) = p_1(x) + p_2(x)$, where $p_1(x) = \exp(-(x_1 + a)^2 - 2x_2^2)$, $p_2(x) = \exp(-(x_1 - a)^2 - 2x_2^2)$, $a \geq 0$, and $x = (x_1, x_2) \in \mathbb{R}^2$. For convenience, we define $\delta(x) = \frac{p_1(x) - p_2(x)}{p(x)}$. Since $\delta(x)$ is actually a function of x_1 , we rewrite $\delta(x)$ as $\delta_*(x_1)$. The gradient*

and Hessian matrix of $f^q \circ p$ are given by

$$\begin{aligned} \nabla(f^q \circ p)(x) &= -2p^q(x) \cdot \begin{bmatrix} x_1 + a\delta(x) \\ 2x_2 \end{bmatrix}, \\ \frac{H_{f^q \circ p}(x)}{4p^q(x)} &= \begin{bmatrix} -\frac{1}{2} + a^2 - a^2\delta_*^2(x_1) & 0 \\ 0 & -1 \end{bmatrix} + q \begin{bmatrix} x_1 + a\delta_*(x_1) \\ 2x_2 \end{bmatrix} \begin{bmatrix} x_1 + a\delta_*(x_1) \\ 2x_2 \end{bmatrix}^T. \end{aligned}$$

When $q = 0$, the Hessian matrix is diagonal with the smallest eigenvalue -1 , where we use the observation that $-1/2 + a^2(1 - \delta_*^2(x_1)) \geq -1/2 > -1$. As a result, the ridge $\mathcal{R}(f^0 \circ p)$ is given by

$$\mathcal{R}(f^0 \circ p) = \{(x_1, 0) \mid x_1 \in \mathbb{R}\}.$$

When $q < 0$, Corollary 6 implies that $\mathcal{R}(f^q \circ p) \subseteq \mathcal{R}(f^0 \circ p)$, and thus we only need to discuss the case where $x_2 = 0$. In this case, the Hessian matrix is again a diagonal matrix and the gradient is parallel to $(1, 0)$. Thus, the ridge $\mathcal{R}(f^q \circ p)$ is given by

$$\mathcal{R}(f^q \circ p) = \{(x_1, 0) \mid 1/2 + a^2(1 - \delta_*^2(x_1)) > -q(x_1 + a\delta_*(x_1))^2, \quad q < 0\}.$$

When $q > 0$, Corollary 6 implies that $\mathcal{R}(f^0 \circ p) \subseteq \mathcal{R}(f^q \circ p)$. Hence, we only need to study the case where $x_2 \neq 0$. First, we study the case where $x_1 + a\delta_*(x_1) \neq 0$ and $x_2 \neq 0$. In this case, $(x_1 + a\delta_*(x_1), 2x_2)$ is not parallel to $(1, 0)$ or $(0, 1)$. Similar to the argument in Example 8, the eigenvectors of $H_{f^q \circ p}(x)$ are not parallel to $\nabla(f^q \circ p)(x)$, and thus $x \notin \mathcal{R}(f^q \circ p)$. Next, we consider the case where $x_1 + a\delta_*(x_1) = 0$. Since $x_1 = 0$ satisfies such equality, the set $\mathcal{S} = \{x_1 \mid x_1 + a\delta_*(x_1) = 0\}$ is non-empty. When x_1 is taken from this set, the Hessian matrix is diagonal with diagonal elements $-\frac{1}{2} + a^2 - x_1^2$ and $-1 + 4qx_2^2$. Thus, it is easy to show that

$$\begin{aligned} &\mathcal{R}(f^q \circ p) \cap \{(x_1, x_2) \mid x_1 \in \mathcal{S}, x_2 \in \mathbb{R}\} \\ &= \{(x_1, x_2) \mid x_1 \in \mathcal{S}, x_2^2 > \frac{1 + 8(a^2 - x_1^2)}{8q}, -\frac{1}{2} + a^2 - x_1^2 < 0\}. \end{aligned}$$

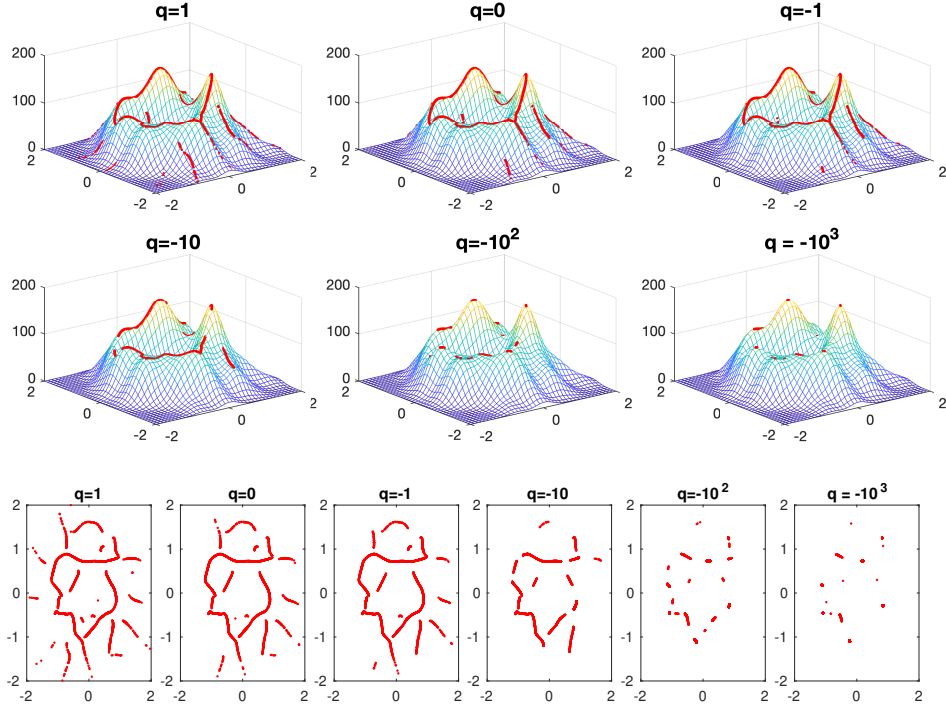


Figure 3: Visualizations of the ridges $\mathcal{R}(f^q \circ p)$, $q \in \{-10^4, -10, -1, 0, 0.5, 1\}$ with $p(x) = \frac{1}{nh^D} \sum_i \exp(-\|x - x_i\|_2^2/h^2)$. The red dots represent the data points obtained from the subspace constrained mean-shift iteration with a bandwidth parameter of $h = 0.3$ in the kernel density function. The blue points represent the underlying truth data.

Combining all the results, we have

$$\begin{aligned} \mathcal{R}(f^q \circ p) &= \{(x_1, x_2) \mid x_1 \in \mathcal{S}, x_2^2 > \frac{1 + 8(a^2 - x_1^2)}{8q}, -\frac{1}{2} + a^2 - x_1^2 < 0\} \\ &\cup \{(x_1, 0) \mid x_1 \in \mathbb{R}\}, \quad 0 < q \leq 1. \end{aligned}$$

Figure 2 provides visualizations of this example.

3.1.2. Ridge estimation with kernel density estimation

In the last example, we present a more general illustration of the transformed ridge by using the kernel density estimation $p(x)$:

$$p(x) = \frac{1}{nh^D} \sum_{i=1}^n \exp(-\|x - x_i\|_2^2/h^2).$$

For ease of notation, let us define the kernel weight $w(x, x_i)$ as follows:

$$w(x, x_i) = \frac{1}{\sum_i \exp(-\|x - x_i\|_2^2/h^2)} \exp(-\|x - x_i\|_2^2/h^2).$$

Using the weight $w(x, i)$, we can denote the weighted-center $c(x)$ as follows:

$$c(x) = \sum_i w(x, x_i) x_i.$$

As the complexity of $f^q \circ p(x)$ makes it challenging to find an analytical representation for $\mathcal{R}(f^q \circ p(x))$, we simplify the ridge condition by deriving the explicit form of the gradient and Hessian matrix for $f^q \circ p(x)$ as follows:

$$\begin{aligned} \nabla p(x) &= \frac{2p^q(x)}{h^2}(c(x) - x), \\ H_{f^q \circ p(x)} &= \frac{4p^q(x)}{h^4}(\Gamma(q, x) - \frac{h^2}{2}I), \end{aligned}$$

where $\Gamma(q, x)$ is a weighted covariance matrix with a rank-1 modification term. Specifically, $\Gamma(q, x) = \sum_i w(x, x_i)(x_i - x)(x_i - x)^T + (q-1)(c(x) - x)(c(x) - x)^T$. The ridge condition is then reduced to:

$$\mathcal{R}(f^q \circ p(x)) = \{x | \Pi^\perp(\Gamma(q, x))c(x) = 0, \lambda_{d+1}(\Gamma(q, x)) < h^2/2\}.$$

We performed a numerical study to investigate variations of ridges using different power transformations via the Subspace Constrained Mean-Shift Algorithm, as shown in Table 1. Visualizations of this example are provided in Figure 3.

4. Numerical Experiments

4.1. SCRE and l -SCRE

The SCRE (Subspace Constrained Ridge Estimation) approach is a framework used to estimate the ridge of a manifold. It involves computing attraction forces and subspaces based on different methods, which may vary across different works. The goal of this section is to demonstrate the effectiveness of the approach in manifold fitting compared to classical subspace-constrained methods. To facilitate the comparison, the general frame is used for all the methods.

Table 1: Subspace Constrained Mean-Shift Algorithm

Input: $X = \{x_1, \dots, x_n\}$; Tolerance parameter: ϵ ; Step size: κ ; Formation of $C(x)$, $\mu(x)$
Output: projected points $Y = \{y_1, \dots, y_n\}$ corresponding to X
For each x_i in X :
(1). Set $x_i(0) = x_i$.
(2). Compute the covariance-like matrix $\Gamma(q, x)$
(3). Apply the eigenvalue decomposition approach to obtain U whose columns consists of the leading d eigenvectors of $\Gamma(q, x)$. Then construct $\Pi^\perp = I_D - UU^T$.
(4). Calculate the attraction force $\mu(x)$.
(5). Move $x_i(t+1) = x_i(t) + \kappa\Pi^\perp\mu(x)$.
(6). Check convergence of $\ x_i(t+1) - x_i(t)\ \leq \epsilon$. If it is satisfied, stop and move to the next sample x_{i+1} , otherwise return to step (2).

Table 2: The construction of the attraction forces and normal subspaces for four approaches

Methods	SCORE	l -SCORE	MFIT-i	MFIT-ii
Component				
Attraction force $\mu(x)$:	$c(x) - x$	$c_I(x) - x$	$\sum_i \alpha_i(x)\Pi_i^\perp(x_i - x)$	$\sum_i \alpha_i(x)(x_i - x)$
Intermediate matrix :	$\Gamma(q)$	$\Gamma_I(q)$	$\sum_i \alpha_i(x)\Pi_i^\perp$	$\sum_i \alpha_i(x)\Pi_i^\perp$
Projection Matrix: Π^\perp	The rank $D - d$ projection matrix $\Pi^\perp = I_D - UU^T$, where the columns of U are the leading eigenvectors of the intermediate matrices.			

The manifold fitting algorithms consist of two main parts. In the first part, an attraction force is generated from a point outside the manifold, directed towards a point near the manifold (often represented by observations). In the second part, the normal space is estimated, and the attraction force is adjusted through projection to align the trajectory of the external point as closely as possible with the projected trajectory. In our uniform frame, we call the matrix which leads to the estimated normal space as the intermediate matrix which can be seen in Table 2. The general frame SCORE algorithm is given in Table 1.

Additionally, a local version of SCORE, denoted as l -SCORE, can be considered. In l -SCORE, instead of using all the samples to compute $\Gamma(q, x)$, an index-based version $\Gamma_I(q, x)$ is defined. Here, I represents the interesting sample index set. If we restrict the set I as a neighborhood samples of x , l -SCORE can be viewed

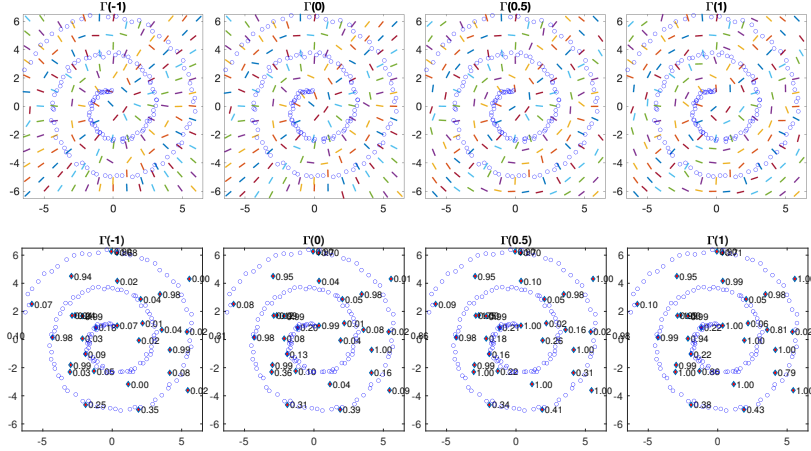


Figure 4: Illustration of the vector field and the value $s(x)$ corresponding to the second eigenvector of $\Gamma(-1, x)$, $\Gamma(0, x)$, $\Gamma(0.5, x)$ and $\Gamma(1, x)$.

as a truncated version of SCORE that excludes distant samples. Specifically, the local version $\Gamma_I(q, x)$ is defined as

$$\Gamma_I(q, x) := \sum_{i \in I} w(x, x_i)(x_i - x)(x_i - x)^T + (q - 1)(c_I(x) - x)(c_I(x) - x)^T.$$

where $\sum_{i \in I} w(x, x_i) = 1$ and $c_I(x) = \sum_{i \in I} w(x, x_i)x_i$. By exclusively focusing on local nearby samples, l -SCORE effectively mitigates the influence of distant samples, resulting in a more refined ridge with improved quality. We list the different versions in Table 2.

Implementation: SCORE, l -SCORE, MFIT-i [21], and MFIT-ii [22]. The MATLAB codes together with all numerical examples used in this paper are available on <https://github.com/zhaizheng/SCORE> (for SCORE, l -SCORE and MFIT-ii). We have implemented MFIT-i, since the authors of [21] have not provided implementation due to the nature of their work has been purely theoretical.

4.2. Ridge Criteria

To validate the effectiveness of the SCORE method, we initially showcase the flow of the projection matrix $\Pi^\perp(x)$ in a 2D swiss-roll toy example. Conse-

quently, a vector flow $u(x) \in \mathbb{R}^2$ exists, where $\Pi^\perp(x) = u(x)u^T(x)$. A reliable estimation of the normal space suggests that $u(x)$ should direct towards the nearest points among the observations. The contrast between the vector flows associated with $\Gamma(-1)$ and $\Gamma(0)$ compared to those associated with $\Gamma(0.5)$ and $\Gamma(1)$ is evident in the initial four diagrams of Figure 4, highlighting the superior performance of the former. In particular, the latter two figures contain erroneous arrows, particularly in areas further away from the sample points.

Intuitively, we can evaluate the extent to which the current x satisfies the ridge condition by using the cosine value of the angle between the gradient and the estimated tangent space as a criterion. Specifically, we define the cosine between the gradient and the estimated tangent space as:

$$s(x) = |\cos(p(x), \Pi(x))| = \|\Pi(x)\nabla p(x)\|_2 / \|\nabla p(x)\|_2,$$

Obviously, if $x \in \mathcal{R}$, the gradient $\nabla p(x)$ is parallel with the estimated tangent space, resulting in a cosine value of ‘1’. Conversely, a lower cosine value indicates the current x is significantly distant from the ridge.

Upon examining the lower four diagrams in Figure 4, several observations come to light. Firstly, the value of $s(x)$ for the same location exhibits a gradual increase from the diagram corresponding to $\Gamma(-1)$ to $\Gamma(1)$. This provides substantiation for our more stringent assertion regarding the ridge condition. Secondly, the magnitude of this increase is more pronounced for locations that are further away from the ridge compared to those in proximity to it. Consequently, we can infer that $\Gamma(-1)$ more precisely captures the geometric characteristics of the ridge in contrast to $\Gamma(0)$.

4.3. Comparison on Synthetic Dataset

We conducted tests on our l -SCRE method using different values of q and compared it with two ridge estimation methods, MFIT-i and MFIT-ii, on synthetic ring and sphere examples. The projection operator onto the ring and sphere manifold was achieved through the normalization process, allowing for convenient computation of the distance between the estimated ridge $\widehat{\mathcal{R}}$ and the

true manifold. To simulate observations, we initially sampled points uniformly on the 1-D circle and the 2-D sphere, denoted as $\tilde{y}_i, i = 1, \dots, m$. Subsequently, we added independent and identically distributed (iid) Gaussian noise to each point $\tilde{y}_i, i = 1, \dots, m$, resulting in the observed points $y_i = \tilde{y}_i + \epsilon_i, i = 1 : m$.

Suppose we obtain the estimated ridge $\hat{\mathcal{R}}$ through l -SCRE MFIT-i or MFIT-ii, we can evaluate the quality of $\hat{\mathcal{R}}$ by computing the Hausdorff distance (Haus) and average margin (Margin) between $\hat{\mathcal{R}}$ and $P_{\mathcal{M}}(\hat{\mathcal{R}})$. These measures are defined as follows:

$$\begin{aligned} \text{Haus}(\hat{\mathcal{R}}, P_{\mathcal{M}}(\hat{\mathcal{R}})) &= \max_{x \in \hat{\mathcal{R}}} \min_{y \in \mathcal{M}} \|x - y\|_2, \\ \text{Marg}(\hat{\mathcal{R}}, P_{\mathcal{M}}(\hat{\mathcal{R}})) &= \frac{1}{|\hat{\mathcal{R}}|} \sum_{x \in \hat{\mathcal{R}}} \min_{y \in \mathcal{M}} \|x - y\|_2. \end{aligned}$$

where $|\hat{\mathcal{R}}|$ is the cardinality of $\hat{\mathcal{R}}$. Here, $\text{Haus}(\hat{\mathcal{R}}, P_{\mathcal{M}}(\hat{\mathcal{R}}))$ represents the maximum distance from any point in $\hat{\mathcal{R}}$ to the nearest point on the manifold \mathcal{M} . On the other hand, $\text{Marg}(\hat{\mathcal{R}}, P_{\mathcal{M}}(\hat{\mathcal{R}}))$ calculates the average distance between points in $\hat{\mathcal{R}}$ and their closest counterparts on the manifold \mathcal{M} .

We begin by examining the influence of the neighbor size on the ridge quality in the case of l -SCRE. Subsequently, we compare the performance of l -SCRE with two other relevant methods. Given that the ridge estimation methods depend on a hyper-parameter h , we conducted a fair comparison by varying h over nine different values, spanning from 0.1 to 0.9.

We draw three key observations from the analysis of Figure 5 and Figure 6. Firstly, in the first two diagrams of Figure 5, it is evident that the ridge associated with $\text{neig} = 30$ is closer to the true manifold compared to the ridge corresponding to $\text{neig} = 100$. This suggests that a smaller neighbor size can yield a more accurate ridge estimation. Secondly, there exists a partial order in terms of ridge quality among $q = -10, -5, 0$, and the performance of $q = -10, \text{neig} = 30$ outperforms all other methods. Lastly, it is worth noting that the l -SCRE method is less influenced by the variation of h , whereas MFIT-i and MFIT-ii demonstrate sensitivity to changes in h . Further details regarding the 1D circle and 2D sphere examples can be found in Table 3.

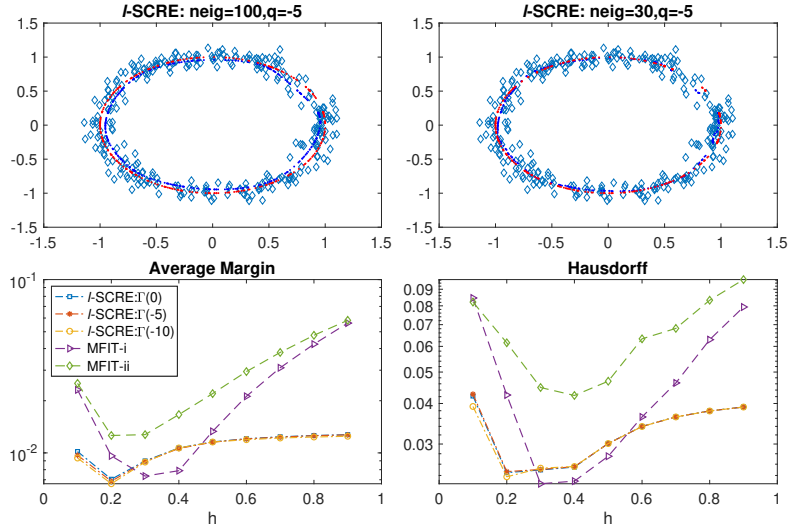


Figure 5: The top two diagrams showcase the obtained ridges and the ground truth manifold for the specific scenarios of $q = -5$ and $\text{neig} = 100, 30$ respectively. The bottom diagrams show the Margin and Hausdorff distance for ridges obtained from l -SCRE and SCRE on the 1D circle.

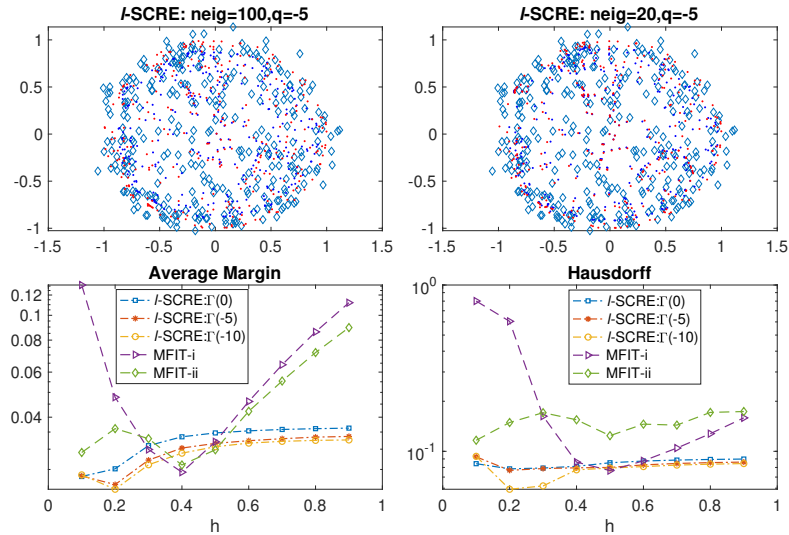


Figure 6: The top two diagrams showcase the obtained ridges and the ground truth manifold for the specific scenarios of $q = -5$ and $\text{neig} = 100, 20$ respectively. The bottom diagrams show the Margin and Hausdorff distance for ridges obtained from l -SCRE and SCRE on the 2-D sphere.

Table 3: The Margin and Hausdorff between $\widehat{\mathcal{G}}$ and \mathcal{M} vary with h for l -SCRE with different q in $\Gamma(\cdot)$ MFIT-i and MFIT-ii on the 1-dimensional circle and 2-dimensional sphere.

		Methods	$\Gamma(\cdot)$	$h = 0.1$	$h = 0.2$	$h = 0.3$	$h = 0.4$	$h = 0.5$	$h = 0.6$	$h = 0.7$	$h = 0.8$	$h = 0.9$
Circle	Marg	l -SCRE	0	0.0102	0.0070	0.0090	0.0107	0.0116	0.0121	0.0124	0.0126	0.0127
		l -SCRE	-5	0.0097	0.0069	0.0089	0.0106	0.0115	0.0120	0.0123	0.0126	0.0127
		l -SCRE	-10	0.0093	0.0066	0.0089	0.0107	0.0116	0.0119	0.0122	0.0123	0.0125
		MFIT-i	-	0.0231	0.0096	0.0073	0.0079	0.0133	0.0212	0.0310	0.0424	0.0561
		MFIT-ii	-	0.0252	0.0126	0.0127	0.0166	0.0220	0.0295	0.0380	0.0477	0.0582
	Haus	l -SCRE	0	0.0422	0.0245	0.0250	0.0255	0.0301	0.0340	0.0364	0.0379	0.0390
		l -SCRE	-5	0.0427	0.0247	0.0250	0.0255	0.0301	0.0340	0.0364	0.0379	0.0390
		l -SCRE	-10	0.0392	0.0238	0.0253	0.0256	0.0301	0.0340	0.0364	0.0379	0.0390
		MFIT-i	-	0.0846	0.0425	0.0226	0.0231	0.0275	0.0364	0.0463	0.0629	0.0793
		MFIT-ii	-	0.0822	0.0615	0.0448	0.0423	0.0468	0.0633	0.0682	0.0833	0.0964
Sphere	Marg	l -SCRE	0	0.0235	0.0251	0.0310	0.0335	0.0347	0.0354	0.0358	0.0361	0.0363
		l -SCRE	-5	0.0236	0.0218	0.0272	0.0303	0.0316	0.0324	0.0330	0.0334	0.0336
		l -SCRE	-10	0.0238	0.0209	0.0261	0.0289	0.0307	0.0317	0.0322	0.0325	0.0326
		MFIT-i	-	0.1313	0.0479	0.0299	0.0244	0.0321	0.0461	0.0641	0.0861	0.1120
		MFIT-ii	-	0.0291	0.0361	0.0330	0.0260	0.0298	0.0422	0.0554	0.0715	0.0895
	Haus	l -SCRE	0	0.0843	0.0784	0.0793	0.0813	0.0853	0.0874	0.0886	0.0893	0.0898
		l -SCRE	-5	0.0927	0.0769	0.0788	0.0796	0.0800	0.0829	0.0845	0.0855	0.0862
		l -SCRE	-10	0.0933	0.0591	0.0619	0.0774	0.0793	0.0810	0.0826	0.0837	0.0844
		MFIT-i	-	0.8011	0.6047	0.1626	0.0861	0.0765	0.0877	0.1046	0.1277	0.1589
		MFIT-ii	-	0.1165	0.1490	0.1707	0.1547	0.1242	0.1457	0.1438	0.1714	0.1735

4.4. Comparison on Real-World Dataset

In addition to evaluating the performance of our algorithm, we conducted tests using the Coil20 dataset, as referenced from the work by [23]. This dataset involves capturing images of an object by rotating it at 360 degrees. Each object in the dataset has 72 images, corresponding to different angles of rotation. Therefore, it can be assumed that the images of each object lie on a one-dimensional manifold, as the only parameter varying is the angle of rotation. However, due to the complexity of the imaging process, the pixel behavior does not exhibit a linear relationship with the angle.

In our study using the dataset Coil20 [23], we consider the images $\tilde{x}_i, i = 1, \dots, m$ as the clean or pure signal and generate observations by adding noise. Specifically, to simulate the corrupted data x_i , we introduce Gaussian noise to the

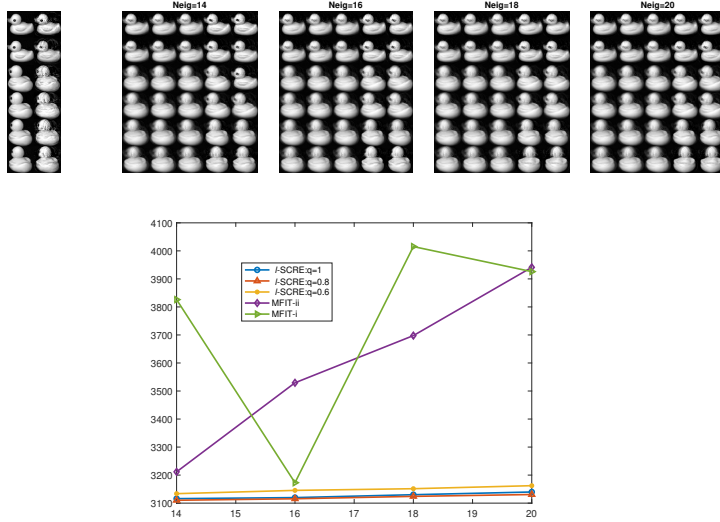


Figure 7: Comparative Analysis of Three Manifold Fitting Algorithms for Denoising. The image depicts the performance comparison of three manifold fitting algorithms in the context of denoising. In the top leftmost figure, the first column represents the original data, while the second column shows the disturbed data in the principal directions. The remaining top four diagrams showcase the recovery images obtained using different algorithms: l -SCORE ($q = 1$), l -SCORE ($q = 0.8$), l -SCORE ($q = 0.6$), MFIT-i, and MFIT-ii. Each algorithm is evaluated with neighborhood sizes ranging from 14 to 20. The bottom diagram illustrates the overall recovery error for the three algorithms, providing an assessment of their performance.

principal directions of each image using the following equation:

$$x_i = U(U^T \tilde{x} + \epsilon_i),$$

Here, U represents a matrix whose columns correspond to the basis vectors associated with the subspace of the most significant variance of the observed data x_i . By applying the above transformation, we effectively project the images onto the lower-dimensional subspace spanned by the columns of U . Consequently, the input for our manifold fitting algorithm becomes the set of projected samples $\{U^T \tilde{x}_i + \epsilon_i, i = 1, \dots, m\}$.

Next, we perform the manifold fitting algorithm on the lower-dimensional subspace. This results in obtaining estimated samples \hat{x}_i corresponding to each

input sample $U^T \tilde{x}_i + \epsilon_i$. To assess the performance and compare different methods, we utilize the mean squared error (MSE) as a criterion. The MSE is calculated as follows:

$$\frac{1}{m} \sum_i \|U^T \tilde{x}_i - \hat{x}_i\|_F^2.$$

This metric quantifies the average squared Frobenius norm of the difference between the projected clean signal $U^T \tilde{x}_i$ and the estimated signal \hat{x}_i . By comparing the MSE values obtained using different methods, we can evaluate their effectiveness in fitting the manifold structure.

We set the parameters as follows: In the l -SCRE method, we vary the hyperparameter h and in the MFIT-i and MFIT-ii methods, we vary the radius r . The values for these parameters are determined using the K -nearest neighbor (KNN) approach such as h or r equal to $\|x - x_{i_K}\|$, where x_{i_K} represents the K -th nearest sample to x . Specifically, we set K to be one of the values in the set $\{14, 16, 18, 20\}$. In addition, for the l -SCRE method, we also vary the parameter q , which controls the degree of the rank-one modification in the local region. The values of q we consider are 0.6, 0.8, 1.

By evaluating the performance of the different methods using the chosen parameter values, as shown in Figure 7, we observe that the l -SCRE method outperforms the other two methods. Furthermore, among the different values of q tested, we find that $q = 0.8$ achieves the best performance for l -SCRE. One advantage of the l -SCRE method is that it primarily focuses on the local region, which makes it less sensitive to changes in the hyperparameter h . This robustness contributes to its superior performance compared to the other methods.

5. Discussion

In conclusion, this study has investigated the impact of nonlinear transformations on ridge estimation and examined the variation of ridges corresponding to different forms. Although the partial inclusion relationship intuitively suggests that leaving some inaccurate branches of the ridges can enhance the quality

of the obtained ridge, a theoretical proof is lacking. While the primary focus of this study has been on improving ridge estimation based on specific distance criteria, it is crucial to acknowledge that other geometric properties, including smoothness and connectivity, are closely associated with ridges and should be taken into account for a more comprehensive understanding.

Looking forward, future research should explore the potential of nonlinear manifold approximation and projection techniques. Existing research has predominantly concentrated on locally approximating the manifold linearly, but incorporating a nonlinear approach that considers curvature information holds promise for achieving more accurate representations of the underlying manifold's geometry over larger regions. By delving into these nonlinear techniques, we aim to advance the field further and enhance the estimation of ridges, thereby deepening our understanding of manifold fitting in the presence of complex data structures.

References

- [1] M. Balasubramanian, E. L. Schwartz, The isomap algorithm and topological stability, *Science* 295 (5552) (2002) 7–7.
- [2] S. T. Roweis, L. K. Saul, Nonlinear dimensionality reduction by locally linear embedding, *science* 290 (5500) (2000) 2323–2326.
- [3] D. L. Donoho, C. Grimes, Hessian eigenmaps: Locally linear embedding techniques for high-dimensional data, *Proceedings of the National Academy of Sciences* 100 (10) (2003) 5591–5596.
- [4] M. Belkin, P. Niyogi, Laplacian eigenmaps for dimensionality reduction and data representation, *Neural computation* 15 (6) (2003) 1373–1396.
- [5] L. Van der Maaten, G. Hinton, Visualizing data using t-sne., *Journal of machine learning research* 9 (11).
- [6] Z. Zhai, H. Chen, Q. Sun, Quadratic matrix factorization with applications to manifold learning, *arXiv preprint arXiv:2301.12965*.

- [7] D. Li, M. Mukhopadhyay, D. B. Dunson, Efficient manifold approximation with spherelets, *Journal of the Royal Statistical Society Series B: Statistical Methodology* 84 (4) (2022) 1129–1149.
- [8] C. Fefferman, S. Mitter, H. Narayanan, Testing the manifold hypothesis, *Journal of the American Mathematical Society* 29 (4) (2016) 983–1049.
- [9] T. Hastie, W. Stuetzle, Principal curves, *Journal of the American Statistical Association* 84 (406) (1989) 502–516.
- [10] V. M. Panaretos, T. Pham, Z. Yao, Principal flows, *Journal of the American Statistical Association* 109 (505) (2014) 424–436.
- [11] U. Ozertem, D. Erdogmus, Locally defined principal curves and surfaces, *Journal of Machine learning research* 12 (Apr) (2011) 1249–1286.
- [12] C. R. Genovese, M. Perone-Pacifico, I. Verdinelli, L. Wasserman, et al., Nonparametric ridge estimation, *The Annals of Statistics* 42 (4) (2014) 1511–1545.
- [13] Y. Y. Tang, H. Yuan, L. Li, Manifold-based sparse representation for hyperspectral image classification, *IEEE Transactions on Geoscience and Remote Sensing* 52 (12) (2014) 7606–7618.
- [14] H. Sasaki, T. Kanamori, A. Hyvärinen, G. Niu, M. Sugiyama, Mode-seeking clustering and density ridge estimation via direct estimation of density-derivative-ratios, *The Journal of Machine Learning Research* 18 (1) (2017) 6626–6672.
- [15] Y.-C. Chen, C. R. Genovese, L. Wasserman, et al., A comprehensive approach to mode clustering, *Electronic Journal of Statistics* 10 (1) (2016) 210–241.
- [16] W. Yao, L. Li, A new regression model: modal linear regression, *Scandinavian Journal of Statistics* 41 (3) (2014) 656–671.

- [17] Y.-C. Chen, Modal regression using kernel density estimation: A review, *Wiley Interdisciplinary Reviews: Computational Statistics* 10 (4) (2018) e1431.
- [18] Y.-C. Chen, C. R. Genovese, R. J. Tibshirani, L. Wasserman, et al., Non-parametric modal regression, *The Annals of Statistics* 44 (2) (2016) 489–514.
- [19] R. A. Horn, C. R. Johnson, *Matrix analysis*, Cambridge university press, 2012.
- [20] Y. Chen, Y. Chi, J. Fan, C. Ma, et al., Spectral methods for data science: A statistical perspective, *Foundations and Trends® in Machine Learning* 14 (5) (2021) 566–806.
- [21] C. Fefferman, S. Ivanov, Y. Korylev, M. Lassas, H. Narayanan, Fitting a putative manifold to noisy data, in: *Conference On Learning Theory*, 2018, pp. 688–720.
- [22] Z. Yao, Y. Xia, Manifold fitting under unbounded noise, arXiv preprint arXiv:1909.10228.
- [23] S. K. N. S. A. Nene, H. Murase, Technical Report CUCS-005-96.